FLOWERING LOCUS T1 is a pleiotropic regulator of reproductive development, longevity, and source–sink relations in barley

Gesa Helmsorig, Tianyu Lan, Einar B Haraldsson, Thea Rütjes, Philipp Westhoff, Katrin Weber, Jochen Kumlehn, Götz Hensel, Rüdiger Simon, Maria von Korff

Plant Physiology, 2026, 200, 1–15
https://doi.org/10.1093/plphys/kiag015
Published: 20 January 2026
Research Article

Plant Physiology® OXFORD

FLOWERING LOCUS T1 is a pleiotropic regulator of reproductive development, longevity, and source–sink relations in barley

Gesa Helmsorig [1†], Tianyu Lan [1†], Einar B. Haraldsson [1], Thea Rütjes [1], Philipp Westhoff [2,3], Katrin Weber[2,3], Jochen Kumlehn [4], Götz Hensel [4,6], Rüdiger Simon [3,5], and Maria von Korff [1,3*]

[1]Institute of Plant Genetics, Heinrich-Heine-Universität Düsseldorf, Düsseldorf 40225, Germany
[2]Institute of Plant Biochemistry, Heinrich-Heine-Universität Düsseldorf, Düsseldorf 40225, Germany
[3]Cluster of Excellence on Plant Sciences "SMART Plants for Tomorrow's Needs", Düsseldorf 40225, Germany
[4]Leibniz Institute of Plant Genetics and Crop Plant Research (IPK), Corrensstr. 3, OT9 Gatersleben, Seeland 06466, Germany
[5]Institute of Developmental Genetics, Heinrich-Heine-Universität Düsseldorf, Düsseldorf 40225, Germany
[6]Present address: Centre for Plant Genome Engineering, Institute of Plant Biochemistry, Heinrich-Heine-Universität Düsseldorf, 40225 Düsseldorf, Germany

*Corresponding author. Maria von Korff., Institute of Plant Genetics, Heinrich-Heine-Universität Düsseldorf, Düsseldorf 40225, Germany. Email: maria.korff.schmising@hhu.de
[†]Contributed equally.
The author responsible for distribution of materials integral to the findings presented in this article in accordance with the policy described in the Instructions for Authors (https://academic.oup.com/plphys/pages/General-Instructions) is Maria von Korff, maria.korff.schmising@hhu.de.

Abstract

Source–sink interactions play a critical but mechanistically underexplored role in coordinating reproductive output and longevity in plants. Here, we investigated the role of *FT1*, the barley (*Hordeum vulgare* L.) homolog of the florigen *FLOWERING LOCUS T* (*FT*), in regulating source (leaf) and sink (inflorescence) development and metabolism. Using *ft1* knockout mutants in the spring barley cultivar Golden Promise, which carries a mutated *PHOTOPERIOD 1* (*ppd-H1*) allele, and in an introgression line with a wild-type *Ppd-H1* allele, we showed that *Ppd-H1* primarily regulates the timing of inflorescence development and flowering through *FT1*. In contrast, variation in tiller number and leaf size was determined by the genetic background. *ft1* mutants exhibited reduced determinacy of both leaf and inflorescence meristems, resulting in increased leaf and spikelet numbers and size, but severely reduced inflorescence fertility, altered senescence patterns, and significantly extended plant longevity. The *ft1* mutants exhibited a strong transcriptional reprogramming of genes involved in both the light and dark reactions of photosynthesis in the leaf, alongside an upregulation of genes associated with carbon catabolism and stress responses in the leaf and inflorescence. Elevated soluble sugar and starch levels in ft1 inflorescences indicated that the impaired development and fertility of *ft1* inflorescences were not caused by carbon limitation, but instead reflected a reduced sink strength. Our work reveals that *FT1* coordinates the development of vegetative and reproductive meristems and organs with plant physiology and metabolism, thereby regulating source–sink relationships and balancing plant longevity with reproductive output.

Introduction

The timing of flowering is a critical determinant of both plant reproductive success and crop yield. Precise coordination of flowering time with environmental conditions is essential to maximize seed set and ensure successful reproduction. At the same time, the developmental timing strongly influences overall shoot and inflorescence architecture and resource allocations, which in turn impact yield potential (Gol et al 2017; Bi et al 2019; Shanmugaraj et al 2023; Dresselhaus et al 2025). The above-ground architecture of a plant is mainly defined by the number, size, and arrangement of organs formed from the shoot apical meristem (SAM) (Benlloch et al 2007). The number of organs developed throughout the lifecycle of a plant depends on the identity and determinacy of shoot meristems. During vegetative growth, the SAM produces leaf primordia and axillary meristems (AXMs) that grow out into leaves and branches, respectively (Wang et al 2018). Reproductive growth is initiated by the irreversible transition of a vegetative SAM into a reproductive inflorescence meristem (IM), which ceases to produce leaf primordia and instead forms floral meristems in eudicots and spikelet meristems (SMs) in grasses (Bommert and Whipple 2018). Meristem determinacy controls how long a meristem remains active and thus the number of organs developed by each meristem type (Bartlett and Thompson 2014). A major gene affecting meristem identity and determinacy in *Arabidopsis thaliana* is *FLOWERING LOCUS T (FT)*, which was

Received: July 11, 2025. **Accepted:** November 25, 2025

identified as the florigen, a mobile floral stimulus that transfers the information to induce flowering from leaves to the developing shoot apex (Chailakhyan 1936; Corbesier et al 2007; Tamaki et al 2007). In flowering-inducing conditions, *FT* is upregulated in phloem companion cells in the vascular tissue of the leaf and transported as a protein through the phloem to the shoot apex (Kardailsky et al 1999; Corbesier et al 2007; Tamaki et al 2007; Chen et al 2018). In the shoot apex, the FT protein interacts with FLOWERING LOCUS D (FD), bridged by 14-3-3 proteins, to form the florigen activation complex (FAC) and activate the expression of floral meristem identity genes and promote floral organ differentiation (Abe et al 2005; Wigge et al 2005; Taoka et al 2011). Through its effects on meristem identity and determinacy, FT controls the length of the vegetative (source-building) phase and thus the number of leaves and potential branches, as well as sink potential, the number of flowers and the size of the inflorescence (Corbesier et al 2007; González-Suárez et al 2023).

FT-like genes have expanded by gene duplications occurring independently in nearly all modern angiosperm lineages, including wheat (*Triticum aestivum* L.) and barley (*Hordeum vulgare* L.), with 12 *FT* paralogs (Chardon and Damerval 2005; Faure et al 2007; Halliwell et al 2016; Bennett and Dixon 2021). In barley, *FLOWERING LOCUS T1* (*FT1*), the major floral inducer, is expressed in the leaves, and high transcript levels of *FT1* are linked to early flowering (Yan et al 2006; Faure et al 2007; Lv et al 2014; Digel et al 2015). *PHOTOPERIOD 1* (*Ppd-H1)* is an upstream regulator of *FT1* orthologous to the *PSEUDO RESPONSE REGULATOR (PRR)* genes of the circadian clock in *Arabidopsis* (Turner et al 2005; Beales et al 2007; Shaw et al 2013). Two major haplotypes have been described in barley, which differ for a nonsynonymous mutation in the conserved CCT (CONSTANS, CO-like, and TOC1) domain (Turner et al 2005). The ancestral wild-type (WT) allele, predominant in wild barley, landraces, and winter barley, is linked to rapid upregulation of *FT1*, floral development, and flowering under long days (LDs) (Turner et al 2005; Digel et al 2015). A mutation in the CCT domain of *Ppd-H1* is associated with delayed and reduced upregulation of *FT1* in the leaf and late flowering under LDs and was selected in spring barley, presumably as an adaptation to long growing seasons in northern cultivation areas (Turner et al 2005; Jones et al 2008). It has been demonstrated that *Ppd-H1* controls leaf size in barley, which is associated with changes in total cell number and the differential regulation of *FT1* in the leaf (Digel et al 2016). However, it is not known if *Ppd-H1* controls flowering time, plant architecture and leaf size only through *FT1* or additional genes and networks. Furthermore, the genetic networks downstream of *FT1* in the leaf and inflorescence and their effects on leaf (source) and inflorescence (sink) development are poorly understood.

In this study, we aimed to dissect the effects of *FT1* on the development of different shoot meristems and organs, and thus on shoot and inflorescence architecture and source–sink relationships during development. We dissected the development of the shoot apical meristem in *ft1* knockout mutants of the spring barley cultivar Golden Promise (GP), with a mutated *ppd-H1* allele and a derived introgression line carrying a wild-type *Ppd-H1*. Furthermore, we analyzed the total transcriptome and carbon metabolites in developing shoot apical meristems and leaves.

ft1 plants were characterized by substantial changes in the determinacy of different shoot and IMs, organ number and size, senescence patterns, and overall plant longevity. The *ft1* mutants exhibited a strong transcriptional reprogramming of genes involved in both the light and dark reactions of photosynthesis, alongside an upregulation of genes associated with sugar catabolism and stress responses. Quantification of soluble sugars and starch in leaves and spikes indicated that the impaired development and growth of *ft1* inflorescences were not due to carbon limitations, but rather to a reduced sink demand, resulting in feedback inhibition of photosynthesis and activation of reactive oxygen species (ROS) scavenging and proteostasis pathways.

Results

FT1 controls the timing of vegetative and reproductive development and plant longevity

Our objective was to investigate how *FT1* affects shoot and inflorescence development in barley, the onset and duration of flowering and transcriptional networks in the leaf and the developing shoot apical meristem. For this purpose, we generated CRISPR-Cas9 induced mutant lines by targeting the coding sequence (CDS) of *FT1* in two different genetic backgrounds: the spring cultivar GP carrying the mutated *ppd-H1* allele and GP-fast, which carries a wild-type (WT) *Ppd-H1* allele introgressed from the winter cultivar Igri (Gol et al 2021; Buchmann et al 2025). We generated 17 independent M2 lines, 14 in GP-fast and three in GP, as confirmed by sequencing the *FT1* locus and scoring for differences in flowering time. Two late-flowering mutants in the background of GP-fast (*ft1.1, ft1.2*) and one late-flowering mutant in the background of GP (*ft1.3*) were chosen for further experiments. These were characterized by a single base pair insertion at position 114 (+T, *ft1.1*), a deletion at position 113 (-C, *ft1.2*), and a deletion at position 88 (-G, *ft1.3*) (Fig. S1a). These indels resulted in frameshifts and premature stop codons, reducing protein length from 177 aa (WT) to 59 aa (*ft1.1*), 60 aa (*ft1.2*), and 29 aa (*ft1.3*) (Figs 1a and S1b). All three *ft1* mutant alleles lacked the DPDxP and GxHR domains conserved in PEBP proteins (Banfield and Brady 2000), segment B, and the LYN triad, which form the external loop crucial for the interaction with bZIP transcription factors (Ahn et al 2006). The truncated *ft1* proteins also lacked the residues Y85 and Q104, important for flowering-activating (Hanzawa et al 2005; Ahn et al 2006) as well as the amino acid residues R62, T66, P94, F101, and R130, which are critical for FT-14-3-3 interactions in wheat and rice (Taoka et al 2011; Li et al 2015) (Fig. 1a). We scored the lines for development and plant architecture traits in two experiments with different pot sizes, small (75 cm^3 wells) and large (1,500 cm^3), that affected development, architecture, and main culm survival.

The parents GP-fast and GP, and the *ft1* mutant lines *ft1.1, ft1.2,* and *ft1.3* were grown in small pots (75 cm^3) under controlled long-day (LD) conditions to determine the effect of *FT1* on flowering time and leaf number of the main culm (Zadoks scale; Zadoks et al 1974), and total tiller number. GP-fast flowered 34 days after emergence (DAE), followed by GP at 48 DAE and the *ft1* mutant lines at 102 DAE (Fig. 1b). While GP-fast with a wild-type *Ppd-H1* allele flowered 14 days before GP with a mutant *ppd-H1* allele, we did not observe significant differences in flowering time among the *ft1* mutant lines in GP-fast versus GP (*ft1.1*: 103 DAE; *ft1.2*: 102 DAE; *ft1.3*: 100 DAE) (Fig. 1b). These observations suggested that *Ppd-H1* acted only or primarily through *FT1* on flowering time. At the onset of flowering, GP plants had produced, on average, 2.1 secondary tillers, not significantly more than the early-flowering GP-fast plants, which produced, on average, 1.7 tillers (Fig. 1c). *ft1* mutants produced significantly more tillers than their respective parent (ft1.1: 4.3; ft1.2: 6.7; ft1.3: 5 tillers) (Fig. 1c). We also investigated whether the extended development in the *ft1* mutants

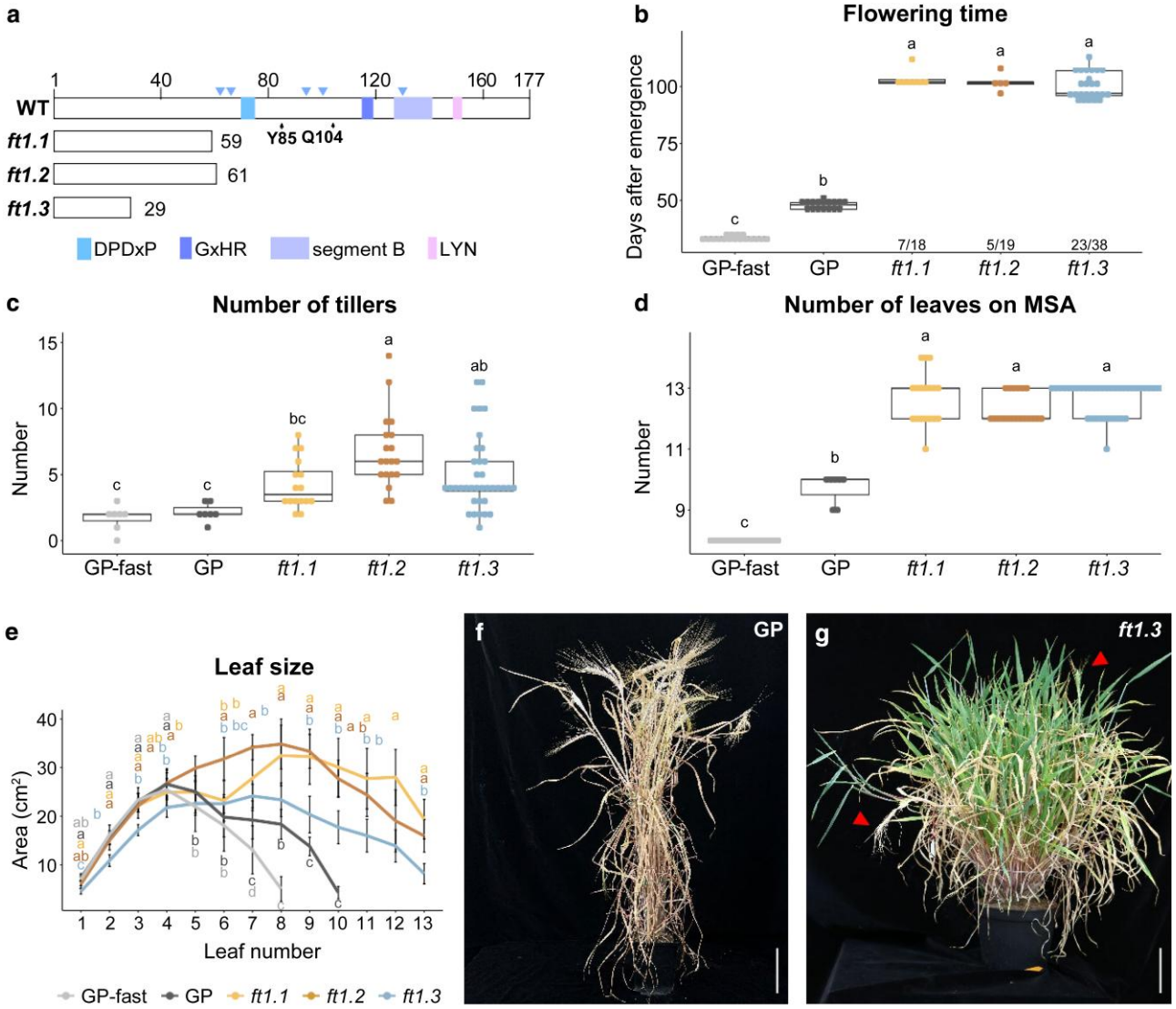

Figure 1 *Ft1* mutant alleles and trait variation. (a) Schematic overview of the FT1 protein sequence in *ft1* mutants *ft1.1*, *ft1.2*, and *ft1.3* compared with wild-type (WT). Residues Y85 and Q104, important for flowering-activating function, are marked (Hanzawa et al 2005; Ahn et al 2006). The boxes represent DPDxP and GxHR domains highly conserved in PEBP proteins (Banfield and Brady 2000), and segment b and the LYN triad, which form the external loop crucial for interaction with a bZIP transcription factor (Ahn et al 2006). Blue triangles indicate the amino acid residues R62, T66, P94, F101, and R130, critical for FT-14-3-3 interactions in wheat and rice (Taoka et al 2011; Li et al 2015). The numbers on the right indicate the protein length of the mutated FT1 proteins. (b–e) GP-fast, GP, and *ft1* mutants were grown under controlled long-day conditions and different traits related to development and plant architecture were scored at flowering (b, c), the end of stem elongation (d), or during development (e). (b) Flowering was scored for the main culm, or, in case the main culm was aborted, for the first tiller ($n = 5$–27). Tiller number (c) was scored from 7 WT plants and 16–36 mutant plants. Each box shows the median and interquartile range (IQR), and whisker lines extend to the smallest and largest values within 1.5*IQR from the lower and upper quartiles, respectively. Outliers beyond this range are represented by individual points. (e) Leaf size was determined by multiplying leaf length and width. Leaf number and leaf size were measured in leaves on the main culm. Error bars indicate the standard deviation of the mean ($n = 10$). Significance levels were determined by one-way ANOVA and subsequent Tukey's test. Different letters above the box and line plots indicate significant differences between groups ($P \leq 0.05$). (f–g) Representative images of a mature GP plant (f) at 4 months after emergence, and a *ft1.3* plant (g) at 10 months after emergence with senescing and newly emerging spikes (red arrows) and green leaves. Scales = 10 cm.

affected the number, size and emergence rate of leaves on the main culm. Leaf numbers on the main culm differed significantly between GP-fast, GP and *ft1* mutants (Fig. 1d). GP-fast produced an average of eight leaves, GP an average of 10 leaves and the *ft1* mutants 13 leaves on the main culm (Fig. 1d). Leaf size increased in the parental lines from leaf one to five and then strongly declined until the flag leaf (Fig. 1e). In contrast, in *ft1* mutants, leaf size increased until leaf nine and then declined, so that the sizes of the last leaves were significantly increased in all *ft1* mutants compared with the parents (Fig. 1e). These size differences were mainly caused by increased leaf lengths in the mutant lines (Fig. S2a, b). The *ft1.3* mutant in the background of GP produced leaves that were significantly smaller and thinner than the leaves of the *ft1.1* and *ft1.2* mutants in the background of GP-fast (Figs 1e and S2a, b). The leaf emergence rates were similar for all genotypes during early development, but started to significantly differ from 18 DAE when emergence rates were fastest in

GP-fast, followed by GP and then the *ft1* mutants (Fig. S2c). The number of visible and green tillers of GP-fast and GP increased until the onset of flowering (Fig. S2d). In contrast, *ft1* mutants continued tillering until 140 DAE when the experiment was stopped (Fig. 1f, g). In the *ft1* mutants, a first wave of tillering was followed by a period of tiller abortion and a second wave of tillering after the onset of flowering (Fig. S2d). The tiller number and emergence rate in *ft1.3* (GP) plants were significantly increased compared with *ft1.1* and *ft1.2* (GP-fast) plants (Fig. S2d).

In a separate experiment, in larger pots (1.5 L), we tested for effects of *FT1* on plant longevity as well as for effects of transformation and tissue culture on development and plant architecture by including null segregant lines (*ft1.1-null, ft1.2-null, ft1.3-null*), sister plants of the *ft1* mutant lines without a mutation event within the *FT1* sequence. We confirmed the differences in flowering time, leaf number and tillering between *ft1* mutants and parental lines and demonstrated that null segregants did not differ from their respective WT parents (Fig. S3a–d). However, in the larger pots, all genotypes produced significantly more tillers, resulting in 100% aborted main culms in the *ft1* plants as compared with 25–75% abortion of main shoots in the smaller pots (75 cm^3) (Fig. S3e, f). However, GP, GP-fast plants, and null mutants were fully senesced at grain maturity after four months, whereas *ft1* mutant plants continued producing new tillers and flowering until the experiment was stopped after 2 years (Fig. 1f, g). The *ft1* mutant plants did not undergo whole-plant senescence, but senescence was restricted to individual tillers. This resulted in plants with many tillers and a high amount of vegetative biomass (Fig. S4).

In summary, *FT1* had pleiotropic effects on flowering time, tillering, leaf development, and plant longevity. All *ft1* mutants flowered at the same time, suggesting that *Ppd-H1* controls time to flowering primarily through *FT1*. In contrast, leaf size and tiller emergence and number at flowering time differed between *ft1.1 and ft1.2* mutants in GP-fast versus *ft1.3* in the GP backgrounds, suggesting that *Ppd-H1* might control leaf size and tillering through other genes than *FT1*. However, the observed differences might also be controlled by other genetic variation than *Ppd-H1* in the introgression line GP-fast (Buchmann et al 2025).

FT1 accelerates the vegetative and reproductive development and increases fertility

To analyze the effects of *FT1* on the developmental subphases of the main shoot apex (MSA), the MSA of GP-fast, GP, and the three mutant lines *ft1.1*, *ft1.2,* and *ft1.3* were dissected during development and scored according to the scale by Waddington et al (1983). In addition to the developmental stage, we scored the number of SMs and floral meristems (FMs), and the inflorescence sizes to calculate the rate of SM initiation, FM development, and FM abortion.

The MSA of GP-fast plants developed significantly faster than that of GP; GP-fast plants transitioned to the double ridge stage (W2.0) at 10 DAE compared with 15.5 DAE in GP and 25 DAE in *ft1* mutant plants (Fig. 2a). The MSA of GP-fast plants showed a linear development across all Waddington stages. In contrast, GP and *ft1* mutants were further delayed during floral development (Fig. 2a). Consequently, GP-fast reached the pollination stage (W10.0) at 38 DAE, GP plants at 52 DAE, and *ft1* plants, on average, at 101 DAE (Fig. 2a). No significant differences in the timing of the developmental subphases, the duration of SM induction, and floral development could be observed among the *ft1* mutants, regardless of their parental background (Fig. 2a). The average rate of SM induction was 0.9 SMs/day in *ft1* mutants and, therefore, strongly reduced compared with the parents with 2.3 SMs/day in GP and 2.9 SMs/day in GP-fast (Table S1). While SMs were induced until the same developmental stage (W4.5–W5.0) in both parents and *ft1* mutant lines, they were induced over a longer time period in the *ft1* mutants and GP due to delayed development (Fig. 2b). Consequently, the maximum SM numbers on the MSA of *ft1* mutants and GP were significantly higher than GP-fast, even though SM induction rates (SMs/day) were reduced (Fig. 2b; Table S1). However, the higher number of SMs did not correlate with an increased inflorescence size, as the inflorescence density (measured in SMs/mm inflorescence) was significantly increased in *ft1* mutants and GP compared with GP-fast (Fig. S5a–c). We then scored floret abortion if SMs or FMs were stalled in development and did not continue to form florets. The total number of SMs/FMs that did not develop into florets was much higher in *ft1* plants compared with parents, with an average of 11.3 aborted SMs or FMs compared with 0.7 in GP-fast and 1.6 in GP on the main spikes (Table S1).

The MSAs of GP-fast, GP, and *ft1* mutants were morphologically similar during vegetative and early reproductive developmental stages (W1.0–W3.0) (Fig. S5d). However, at the stamen primordium stage (W3.5), secondary inflorescences started to emerge from the basal central SMs of the MSA in *ft1* plants, but not in the parental plants (Fig. 2c). We observed this in 60–80% of the dissected main culms of *ft1* plants. This usually occurred only on one side of the inflorescences, and in rarer cases (about 10%) on both sides. Compared with the MSA, the secondary inflorescences were delayed but appeared to develop normally. They resulted in branched spikes at the base of the spike (Fig. S6).

Next, we evaluated the effect of *FT1* on the number of spike-bearing tillers and the number of florets and grains on the main spike. The floret number was significantly higher in GP than in GP-fast, while the grain number per main spike was not significantly different between the two genotypes (Fig. 2d, e). In *ft1* mutants, the floret number was increased compared with GP-fast but not to GP (Fig. 2d). Spike fertility, the number of grains per floret on the main spike, ranged from 0% to 15% in *ft1* mutant plants and was thus significantly lower than in GP-fast (90%) and GP (70%) (Fig. 2f). The tiller fertility, the ratio of spike-bearing tillers with at least one grain versus the total number of tillers, was close to 100% in GP-fast and GP (Fig. 2g). In contrast, tiller fertility of *ft1.1*, *ft1.2,* and *ft1.3* was significantly lower, averaging only 20%, 29%, and 44%, respectively (Fig. 2g). Compared with GP-fast and GP, *ft1* mutant plants produced normal ovules but smaller anthers with fewer and shriveled nonviable pollen, as demonstrated by pollen viability testing and electron microscope imaging (Figs 2h, i and S7). Based on these measurements, pollen viability was reduced significantly from 96% to 97% in GP-fast and GP to an average of 81%, 78%, and 88% in *ft1.1*, *ft1.2,* and *ft1.3*, respectively (Fig. 2i). We thus concluded that the impaired anther and pollen development contributed to the reduction in floret fertility in the *ft1* mutant plants. *FT1* also affected grain morphology as thousand-grain weight (TGW) and two-dimensional grain area were significantly reduced in *ft1* mutants compared with the parents, mainly due to reduced grain width (Figs 2j and S8).

In conclusion, *ft1* mutants were characterized by delayed reproductive development, slower but longer SM and FM induction, and increased floret abortion, which resulted in a strong reduction in the number of grains per main spike compared with the parents. This caused a reduced spike fertility, likely affected by a reduced pollen

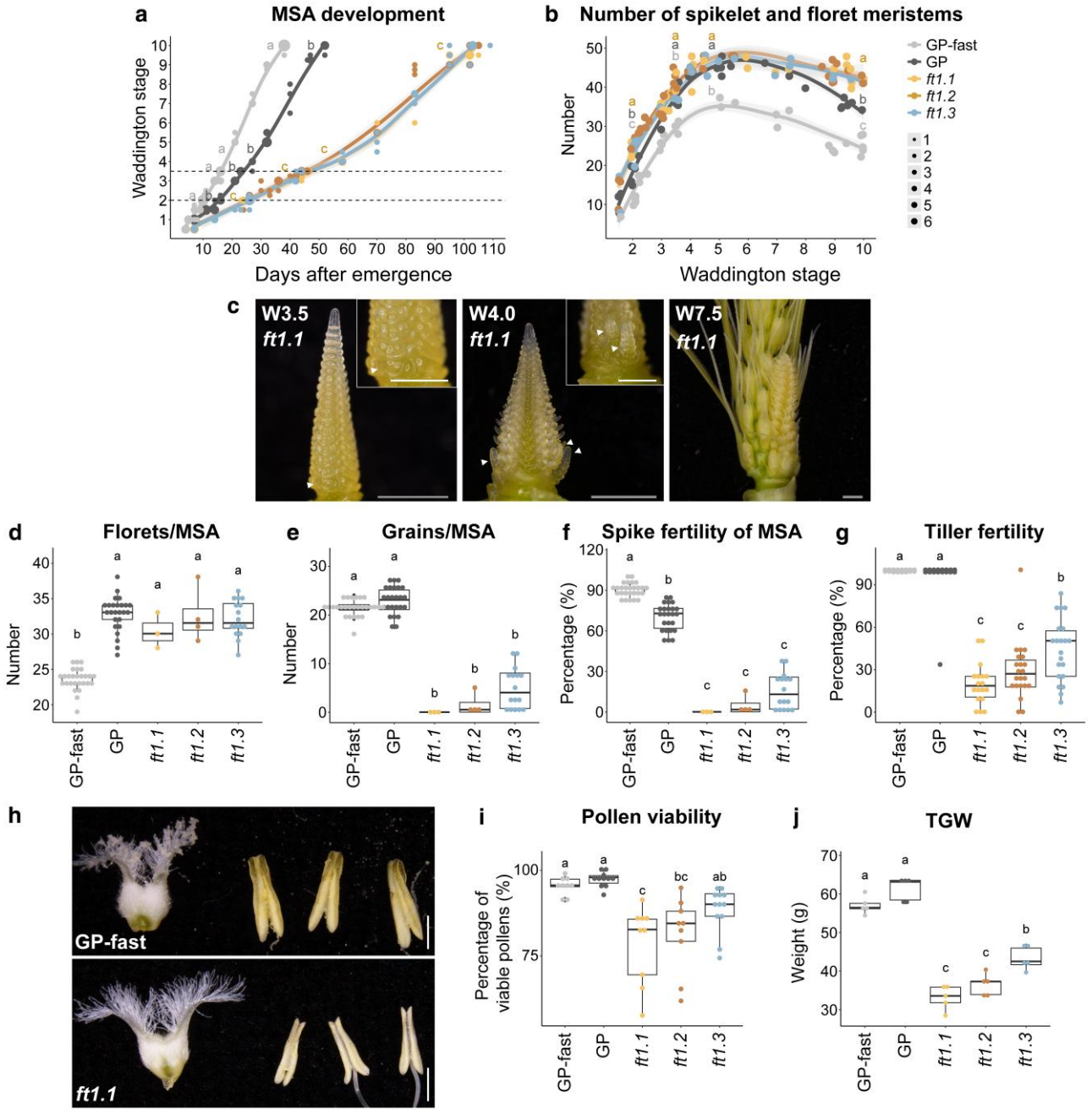

Figure 2 Effects of *FT1* on reproductive development. (a–d) The main shoot apex (MSA) development was monitored from 4 days after emergence to flowering on the main culm of GP-fast, GP, and *ft1* mutants. (a) Development of the MSA according to the scale by Waddington et al (1983). Dot sizes indicate the number of plants per data point (1–6), and gray areas show the 95% confidence interval of a polynomial regression (Loess smooth line). The dotted lines indicate the transition from vegetative to reproductive growth (W2.0) and to floral development (W3.5). (b) Number of spikelet and floret meristems on the MSA. Significance levels in (a) and (b) were determined by one-way ANOVA and subsequent Tukey's test ($P \leq 0.05$) at developmental stages W2.0, W3.5, W4.5/W5.0, and W10.0. Values from *ft1* mutants were combined and compared with GP-fast and GP. The colors of the characters indicate the respective group (light gray: GP-fast, dark gray: GP, orange: mutants). (c) Representative MSA of *ft1.1* plants during floral development (W3.5 to W7.5). White arrows indicate secondary inflorescences at the base of the primary inflorescence. A small image in the top right shows the magnified view of the same MSA from a different angle. White scale bars = 500 μm, gray scale bars = 1,000 μm. (d–g) Reproductive traits in *ft1* plants. Floret number (d), grain number (e), and floret fertility (f) were scored on the main culm. Floret fertility was calculated by dividing the number of grains by the number of florets ($n = 3$–27). Tiller fertility was determined by dividing the number of tillers with a spike that holds at least one seed by the final tiller number ($n = 18$–27). Each box shows the median and interquartile range (IQR), and whisker lines extend to the smallest and largest values within 1.5*IQR from the lower and upper quartiles, respectively. Outliers beyond this range are represented by individual points. (h) Representative images of GP-fast and *ft1*.1 ovules and anthers; scales = 1,000 μm. (i) Pollen viability, with values averaged for each floret ($n = 8$–23). (j) Thousand-grain weight (TGW) was measured with five biological replicates, each containing pooled grains from three individual plants ($n = 5$). Significance levels were determined by one-way ANOVA and subsequent Tukey's test. Different letters above the boxplots indicate significant differences between groups ($P \leq 0.05$).

number and viability. Spike architecture in *ft1* plants was altered by the outgrowth of secondary inflorescences from the basal central SMs, resulting in branched spikes. The extended leaf growth, IM activity, and plant longevity observed in the *ft1* mutant lines suggest that *FT1* plays a critical role in establishing the determinacy of various meristem types, thereby coordinating vegetative and reproductive development and ultimately maintaining source–sink homeostasis.

FT1 affects the expression of genes involved in stress response, chromatin remodeling, and carbon metabolism

To identify genes and genetic networks underlying the *FT1*-controlled phenotypes, we conducted transcriptome profiling in *ft1* mutants, GP, and GP-fast. For this purpose, we harvested leaves and MSAs at key reproductive stages: the initiation of spikelet development (W2.0), the onset of floral development (W3.5), and the end of spikelet induction (W5.0).

Principal component analyses (PCA) of the leaf and MSA transcriptome data demonstrated that PC1 separated the genotypes, whereas PC2 separated the developmental stages for leaf and MSA samples, while the genotype and stage-dependent clusters were more pronounced in MSA than leaf samples (Figs S9a and S10a). GP with low *FT1* expression levels exhibited transcriptional profiles intermediate between those of the mutants with nonfunctional *ft1* and GP-fast, characterized by a strong induction of *FT1* expression (Figs S10a and S11). We focused our transcriptome analysis on *FT1*-dependent effects, as we found no significant developmental differences in the timing of MSA development and flowering among the *ft1* mutants and wanted to exclude possible effects caused by the background introgression in GP-fast (Figs 1c and 2a). We thus identified differentially expressed genes (DEGs) that were consistently regulated across all three *ft1* mutants relative to their respective parental lines at the same stage. We identified a total of 646 and 628 DEGs in leaf and MSA, respectively (Fig. 3a, b; Datasets S1, S2). In the leaf, 395 DEGs were upregulated and 251 downregulated, and in the MSA, 396 transcripts were upregulated and 232 downregulated in the *ft1* mutants (Fig. 3a, b). The number of DEGs increased in both tissues with the developmental stage (Fig. 3a, b). Only 40 DEGs overlapped between leaf and MSA tissues, which included the developmental genes *ODDSOC1* (*HvMADS25*), *AGL14*, and the starch-degrading enzyme *BETA-AMYLASE*, which were strongly upregulated in both leaf and MSA in *ft1* mutants (Figs S11 and S12).

To identify coexpression clusters correlated to genetic and expression variation of FT1, the timing of MSA development and spikelet primordium (SP) and FM induction, a weighted gene coexpression network analysis (WGCNA) was performed in the leaf and MSA, respectively (Figs 3c, d and S13). We identified five coexpression clusters in the leaf and ten in the MSA. Coexpression clusters with transcripts upregulated in the *ft1* mutants were enriched for functions in stress response in both leaf and MSA, and for functions in transcription and translation only in the MSA (Figs 3e, f and S9b, S10b). Coexpression clusters downregulated in the *ft1* mutants were enriched for functions in photosynthesis and carbon metabolism in the leaf and MSA, and for chromatin remodeling only in the MSA (Figs 3e, f and S9b, S10b; Datasets S3, S4).

In the leaf, coexpression module L2 (325 DEGs), with the strongest positive correlation to the timing of MSA development and negative correlation to FT1, included 79 genes with putative functions in the mitigation of oxidative stress (reactive oxygen species (ROS) scavengers, *CATALASE*), heavy metal toxicity (*HEAVY METAL TRANSPORT/DETOXIFICATION SUPERFAMILY PROTEINS* [*DTX*], *ABC TRANSPORTER*s), heat (*HEAT SHOCK PROTEIN*s [*HSP*s]) and pathogens (*HYPERSENSITIVE-INDUCED RESPONSE PROTEIN* [*HIR*]), *NBS-LRR*s) (Figs 3c, e and S11; Dataset S1). In addition, 143 genes were associated with metabolic adjustment and stress-related signaling pathways. These included kinases (*SERINE/THREONINE* [*Ser/Thr*] kinases, *RECEPTOR-LIKE KINASES* [*RLK*s]), *PHOSPHATASE* 2C genes (*PP2C*s), transcription factors (*WRKY*, *NAC*, *MYB*, *bZIP*, and *bHLH* families), transporters (*SUGAR TRANSPORTER* genes, *PHOSPHATE TRANSPORTER 1*, and *NRT/PTR* family transporters), as well as enzymes (*FRUCTOKINASE FRK2 KINASE*, *BETA-AMYLASE*, *GLYCOSYLTRANSFERASE, BETA-GLUCOSIDASE*) involved in carbon catabolism under stress conditions (Figs 3e and S11; Dataset S1). In addition, the floral repressor *FT4* and developmental regulator *AGL20* were strongly upregulated in the *ft1* mutant plants but were not or lowly expressed in GP and GP-fast (Figs 3e and S11) (Pieper et al 2021). In contrast, leaf module L4 (171 DEGs), which showed the strongest negative correlation with the timing of MSA development, was enriched for genes involved in photosynthesis and carbon fixation (Figs 3e and S9b). Specifically, *CHLOROPHYLL A-B BINDING* (*CAB*) genes, *PHOTOSYSTEM I SUBUNIT* genes (*PsaO*, *PsaE-2*), *PHOTOSYSTEM II SUBUNIT* genes (*PsbR*, *PsbW*), *RIBULOSE BISPHOSPHATE CARBOXYLASE SMALL CHAIN 1A* (*RBCS1A*) genes, *RUBISCO ACTIVASE* (*RCA*), and *D-RIBULOSE-5-PHOSPHATE-3-EPIMERASE* (*RPE*) gene were downregulated in the *ft1* mutants (Fig. S11; Dataset S1). These results showed that coexpression clusters in the leaf associated with FT1 function and MSA development were enriched for functions in stress responses, photosynthesis, and carbon metabolism.

In the MSA, modules M1–M7 comprising 396 DEGs upregulated in the *ft1* mutant, were, like the leaf modules L1-L3, enriched for stress response genes, such as heat stress responses (*HEAT SHOCK FACTOR*s [*HSF*s], *HSP*s), ROS scavenging (*GLUTATHIONE TRANSFERASE*s [*GST*s], *GLUTAREDOXIN*, *LIPOXYGENASE*s), hormonal stress signaling (*ETHYLEN-RESPONSIVE TRANSCRIPTION FACTOR*s [*ERF*s], *JASMONATE-RESPONSIVE PROTEIN*s, *AUXIN RESPONSE FACTOR 1* [*ARF1*], *PP2C*), detoxification (*DTX*s), ubiquitin-mediated protein turnover (*F-BOX* proteins, *POLYUBIQUITIN*), metabolic stress or starvation responses (*PYRUVATE DECARBOXYLASE*, *PHOSPHOGLYCERATE KINASE*), fatty acid oxidation enzymes, (*HEXOSYLTRANSFERASE*s), and programmed cell death (*DEVELOPMENTAL AND CELL DEATH* gene [*DCD*]) (Figs 3f and S12; Dataset S2). Additionally, DEGs in M1–M7 were enriched for functions in transcriptional and posttranscriptional regulation (*TRANSCRIPTION ELONGATION FACTOR TFIIS*, *TRANSLATION ELONGATION FACTOR 1-α*, *SPLICING FACTOR*s), and for transposable elements (CACTA, *RETROVIRUS-RELATED* POL *POLYPROTEIN*s), indicating elevated transcriptional activity in *ft1* MSAs (Figs 3f and S12; Dataset S2). Moreover, the expression of *MADS-box* gene *ODDSOC2*, flowering repressor *CONSTANT 9-LIKE*, and circadian clock gene *PRR73/PRR95*, were strongly upregulated in the MSA of *ft1* mutants (Fig. S12; Dataset S2). Notably, modules M1–M7 were negatively correlated with SP numbers and rate of SP initiation, suggesting that delayed SP and FM development was linked to molecular stress response and transcriptional reprogramming in the MSA (Figs 2a and 3d). In contrast, three modules (M8–M10) were negatively correlated with the genetic and expression variation of *FT1* in the leaf. These modules included the *FT1* paralog *FT2*, *MADS-box* transcription

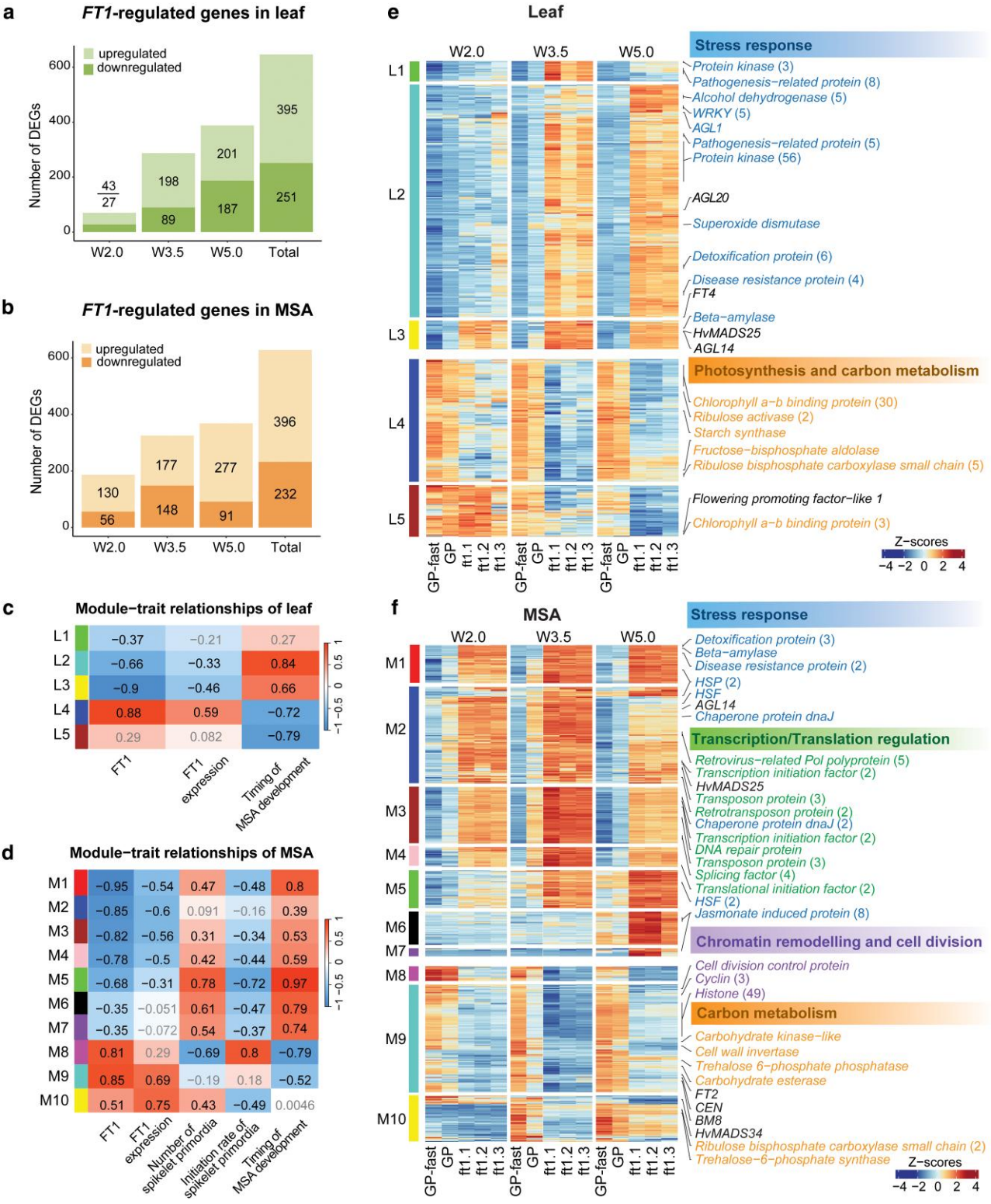

Figure 3 Effects of *FT1* on transcriptomic changes in leaf and inflorescence. (a–b) The number of differentially-expressed genes (DEGs) regulated by *FT1* at each developmental stage and in total across all stages in the leaf (a) and main shoot apex (MSA). Genes that were either up- or downregulated in all *ft1* mutants (*ft1.1 vs.* GP-fast, *ft1.2 vs.* GP-fast, and *ft1.3 vs.* GP) at the same stage were considered as *FT1*-regulated genes. (c–d) Correlation between *FT1*-regulated genes and genetic and phenotypic traits. L1-5 are modules identified in leaf (c), and M1-10 are modules in MSA (d). Values in the cell represent the correlation coefficient. Gray values show nonsignificant correlations. The color scale on the right side indicates the strength and direction of the correlation. Details can be found in Fig. S13. (e–f) The heatmaps show the transcript profiles of genes in each module. Top gene ontology (GO) terms for modules are shown on the side of the heatmap with representative genes in the GO terms. Genes involved in stress response (blue), photosynthesis and carbon metabolism (orange), transcription and translation regulation (green), and chromatin remodeling (purple) are labeled next to their transcript heatmaps. Details can be found in Datasets S1 and S2. The color scale represents the range of *Z*-score normalized mean transcript per million (TPM) of three biological replicates.

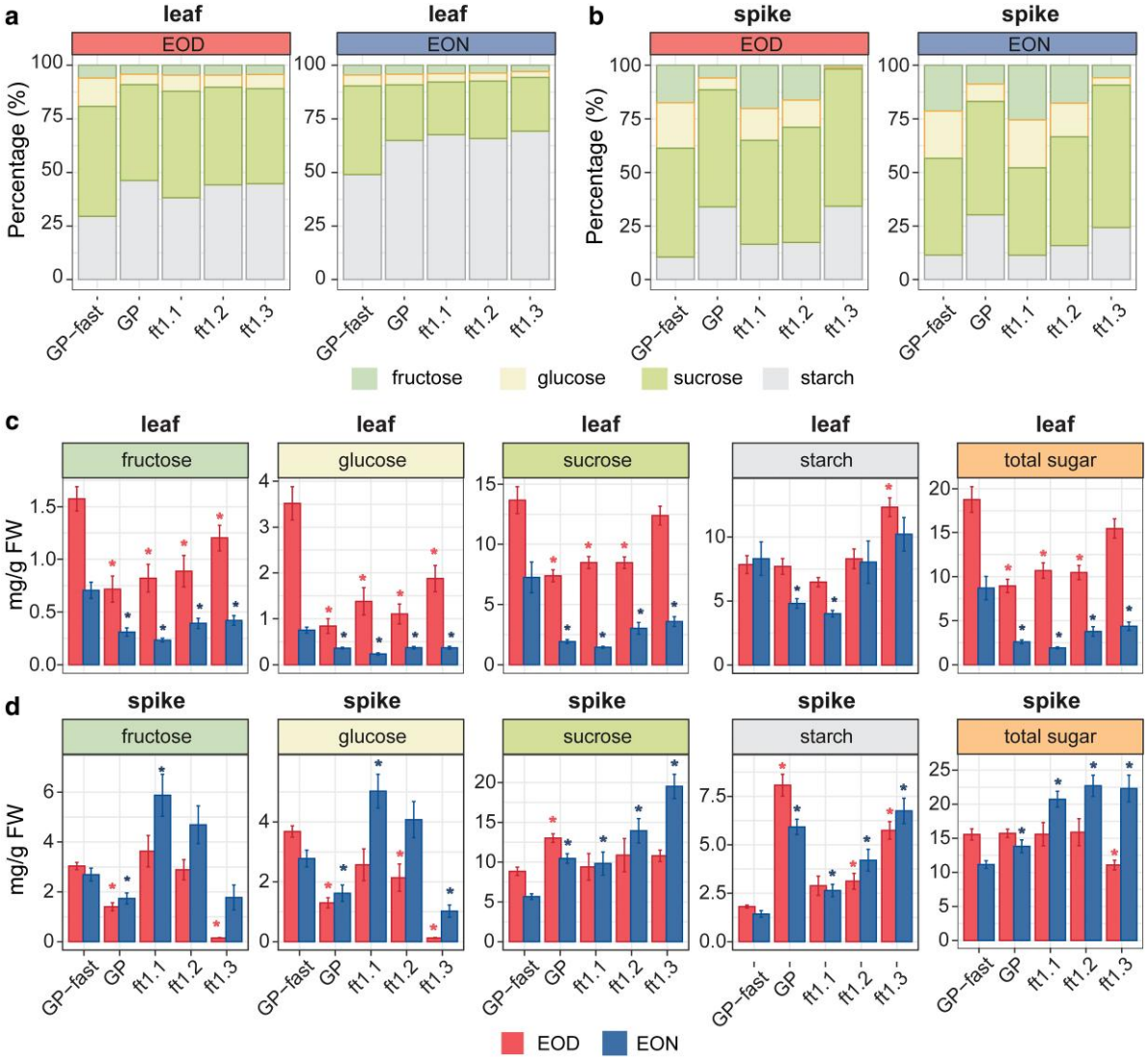

Figure 4 Effect of *FT1* on soluble sugars and starch content in the leaf and spike. (a–b) Proportion of soluble sugars and starch in the leaf (a) at 16 days after emergence and in the spike (b) at developmental stage W8.0–8.5 (before pollination) of GP-fast, GP, *ft1.1*, *ft1.2* and *ft1.3* at the end of day (ZT 16; EOD) and the end of night (ZT 0; EON). (c–d) Soluble sugars and starch content in leaves (c) and spikes (d) at EOD (red) and EON (blue). FW, fresh weight. Error bars indicate the standard error of 10 biological replicates. Significance levels were determined by comparing GP or *ft1* mutants to GP-fast at either EOD or EON using Fisher's *F*-test for homoscedasticity, followed by Welch's *t*-statistic. Red asterisks indicate significant differences at EOD, blue asterisks at EON. *, $P \leq 0.05$.

factors *CENTRORADIALIS* (*CEN*) and *BM8*, which promote floral development and floret fertility; and genes associated with chromatin remodeling and cell division, such as *HISTONE* and *CYCLIN* family members (Figs 3f and S12; Dataset S2). Moreover, modules M8–M10 were enriched for genes involved in carbon metabolism and signaling, including *TREHALOSE-6-PHOSPHATE SYNTHASE 1* (*TPS1*) and *TREHALOSE-6-PHOSPHATE PHOSPHATASE G* (*TPPG*), two enzymes that act sequentially to regulate the trehalose-6-phosphate (T6P) balance, as well as *CELL WALL INVERTASE 2* (*CWINV2*), which controls sucrose cleavage in sink tissues (Fig. S12).

Taken together, the delay in MSA development and decrease in SP and FM induction rates in the *ft1* mutants were linked to a transcriptional stress response and downregulation of transcripts involved in floral development and in carbon assimilation and signaling in leaves and MSA.

FT1 affects soluble sugar and starch levels in the leaf and spike

We then tested if the *FT1*-dependent regulation of photosynthesis-related genes in the leaf and of carbon signaling and metabolism in the MSA was linked to carbon availability. Therefore, we measured starch and soluble sugars at the end of the day (EOD) and end of the night (EON) in leaves and MSAs at the pre-anthesis stage (W8.0–W8.5). In the leaf, sucrose was most abundant, followed by starch, glucose, and fructose at the EOD, while starch levels were relatively higher than sucrose at EON (Fig. 4a). In the spike, sucrose was more abundant than starch, followed by glucose and fructose at EOD and EON (Fig. 4b). In the leaf, GP-fast accumulated higher levels of sucrose, glucose, and fructose, particularly at EOD, compared with GP and the *ft1* mutants, while GP and *ft1* mutants did not differ for these metabolites in the leaf (Fig. 4c). Leaf starch levels were consistently different between GP-fast versus GP and *ft1* mutants at

EOD or EON (Figs 4c and S14a). In the spike, GP and the *ft1* mutants had higher levels of sucrose and starch at EOD and EON compared with GP-fast (Fig. 4d). Furthermore, all three *ft1* mutants displayed higher fructose, glucose and total sugar levels at EON than EOD, while GP-fast and GP sugar levels were not different or lower at EON than EOD in the spike (Figs 4d and S14b).

Taken together, *ft1* mutant plants showed reduced levels of soluble sugars in the leaf, but increased sucrose and starch in the inflorescence compared with GP-fast, as well as higher fructose, glucose and total sugar levels in the spike at EON than EOD.

Discussion

FT1 coordinates source–sink growth

Loss of a functional FT1 protein not only delayed the transition from vegetative to reproductive development but also slowed down and extended the period of reproductive growth (Fig. 1g, 2a). In all three *ft1* mutant lines, the transition to reproductive development and the timing of reproductive phases were consistently delayed, irrespective of the allelic state of *Ppd-H1*, indicating that *Ppd-H1* regulates MSA development primarily via FT1 (Fig. 2). However, leaf size and tiller number at flowering time differed between *ft1.1* and *ft1.2* mutants in the GP-fast background versus *ft1.3* in the GP background, suggesting that *Ppd-H1* or other variants introgressed from Igri into GP-fast might control these traits (Figs 1, 2, 4, and S15).

In all *ft1* mutants, prolonged vegetative development led to the formation of more leaf primordia, increased leaf numbers, and enhanced tillering, thereby increasing source strength (Fig. 1). Similarly, the prolonged activity of the IM resulted in an extended period of spikelet initiation and an increased number of spikelets on the main inflorescence (Fig. 2). In addition, basal central SMs reverted into secondary IMs, giving rise to a branched spike architecture (Figs 2 and S6). The reversion of SMs to secondary inflorescences was also observed in the barley *mnd1* mutant and wheat and barley lines, with high expression levels of *SHORT VEGETATIVE PHASE 1* (*SVP1*)-like genes (Trevaskis et al 2007; Walla et al 2020; Li et al 2021). Similarly, the upregulation of the *SVP-like* gene *ODDSOC1* (*HvMADS25*) in the leaf and the inflorescence was linked to floral reversion in the *ft1* mutants (Figs 2, S11, and S12). Furthermore, the downregulation of floral homeotic genes such as *FT2* and *BM8*, which are associated with floral organ development in wheat and barley (Digel et al 2015; Mulki et al 2018; Shaw et al 2019), correlated with the arrested floral development and pronounced reduction in grain number per spike in the *ft1* mutant lines (Figs 2 and S12). Consequently, sink strength was strongly reduced in *ft1* mutant plants despite an increase in spikelet primordia numbers during early reproductive growth.

The *ft1* mutants exhibited prolonged leaf development. Previous work identified *Ppd-H1* as a major determinant of leaf size in barley (Digel et al 2016). Our findings suggest that *Ppd-H1* influences leaf size by regulating *FT1* expression in leaves. *FT1* may affect leaf size either directly, by modulating leaf determinacy and cell proliferation, or indirectly, by altering the timing of inflorescence development and thus stem elongation (Fig. 2). The latter is closely linked to the phyllochron, the interval between the emergence of successive leaves, which determines how long a leaf can grow before the next leaf emerges (Digel et al 2016) (Fig. S2). Additionally, *ft1* plants exhibited increased tillering. Similar effects of *FT* homolog knockouts on branching have been reported in other plant species. In wheat, loss-of-function or deletion of the *FT-B1* allele resulted in increased leaf and tiller numbers (Dixon et al 2018; Finnegan et al 2018). In tomato, mutations in *SFT*, the *FT* ortholog, enhance leaf production and branching (Park et al 2014). Likewise, *Cas9-GhFT* plants in cotton exhibit indeterminate meristem growth and altered branching architecture (Sang et al 2025).

The *ft1* mutants exhibited prolonged tillering over many months and lacked whole-plant senescence, suggesting that *FT1* controls not only the onset, but also the duration of flowering and plant longevity (Figs 1, S3, and S4). This growth habit is reminiscent of perennial plants, which do not undergo whole-plant senescence but maintain undifferentiated meristems (Albani and Coupland 2010). Similarly, Melzer et al (2008) showed that the downregulation of flowering time inducers in annual *Arabidopsis* resulted in plants with recurrent growth cycles and markedly increased longevity. Recent studies in *A. thaliana* have shown that flowering time genes regulate not only the initiation but also the duration and termination of flowering (Balanzà et al 2018; Miryeganeh 2021; González-Suárez et al 2023). Consistent with this, our findings suggest that *FT1* controls both the onset and duration of flowering, as well as senescence patterns, thereby influencing overall plant longevity in barley.

Reduced sink growth is linked to a feedback inhibition of photosynthesis genes, and activation of stress response pathways

The changes in source–sink tissues observed in *ft1* mutant lines were accompanied by extensive transcriptional reprogramming, the downregulation of genes involved in both the light and dark reactions of photosynthesis, as well as the upregulation of genes associated with sugar catabolism and stress responses (Fig. 3; Datasets S1, S2). Specifically, transcripts encoding photosystem components and RuBisCO subunits were reduced, while genes involved in starch breakdown and the utilization of cell wall-derived sugars were upregulated (Figs S11 and S12). Accordingly, soluble sugars, particularly sucrose, were reduced in the *ft1* mutant leaves. In contrast, sucrose and starch levels were rather increased in *ft1* mutant spikes compared with GP-fast. Specifically, the increase of fructose and glucose at EON compared with EOD in the MSA likely reflected reduced carbon use caused by impaired spike development and growth, as indicated by the downregulation of cell cycle genes in *ft1* inflorescences (Fig. 4). Furthermore, low *TPS1* expression likely reflected reduced T6P signaling, thereby promoting sugar breakdown as seen in the strong upregulation of *BETA-AMYLASE* expression and suppressing growth processes (Fichtner and Lunn 2021; Kumar et al 2023) (Fig. S11). These results suggest that the delayed growth and development of *ft1* inflorescences were not caused by carbon limitations, but rather by changes in development and growth, and thus sink strength.

Among the most striking molecular alterations observed in *ft1* mutants was the pronounced upregulation of stress-response genes in both leaf and MSAs tissues (Fig. 3; Datasets S1, S2). The upregulation of *CHAPERONEs* and *HSPs*, together with genes involved in reactive oxygen scavenging, and in ubiquitin-mediated protein turnover, was a strong indicator of the unfolded protein response (UPR), reflecting cellular stress due to misfolded proteins and activation of proteostasis pathways (Sewelam et al 2016) (Fig. 3; Datasets S1, S2). Concurrently, the downregulation of *HISTONE* genes and upregulation of transcripts related to transcription and translation suggested active chromatin remodeling, likely facilitating enhanced access to and transcription of stress-responsive genes in the inflorescence

(Fig. 3; Dataset S2). The observed transcriptional stress signature mirrored the molecular responses reported in *Arabidopsis* and barley shoot apical meristems under high-temperature conditions, where strong induction of HSFs and HSPs was observed (Ejaz and von Korff 2017; Olas et al 2021; John et al 2022, 2024; Lan et al 2025). In rice, the photoperiod regulator *HEADING DATE 1 (Hd1)*, an upstream activator of FT under long-day (LD) conditions, has been implicated in modulating salt stress sensitivity, suggesting that photoperiodic flowering regulators may play broader roles in abiotic stress adaptation (Biancucci et al 2025). On the other hand, it has been demonstrated that low sink demand can lead to the downregulation of the photosynthetic machinery and the generation of ROS, which in turn triggers the induction of protective mechanisms, such as antioxidant enzymes, to prevent damage (Paul and Foyer 2001; Lv et al 2020). We thus speculate that an increase in photosynthetically active source tissue and a reduction in sink tissue in the *ft1* mutant plants might have caused a metabolic feedback inhibition of photosynthesis genes and activation of stress signaling pathways.

Our work reveals that *FT1* coordinates the development of vegetative and reproductive meristems and organs with plant physiology and metabolism, thereby regulating source–sink relationships and balancing plant longevity with reproductive output. Identification and characterization of metabolites and signals controlling the *FT1*-dependent source–sink changes will be important for manipulating the relationship between plant longevity and reproductive output.

Materials and methods

Plant material

Spring cultivar GP (carrying a mutated *ppd-H1* allele) and its derived introgression line GP-fast (wild-type *Ppd-H1* introgressed into GP from Igri; Gol et al 2021; Fig. S15) were transformed using a method previously described (Marthe et al 2015) with an FT1-specific guide (CRISPR-g)RNA/Cas9 construct (pGH465, Fig. S16) that directly derives from the generic binary vector pSH121 (Gerasimova et al 2018) to create plants with a nonfunctional *FT1 (HORVU.MOREX.r3.7HG0653910)* gene. The sgRNA targeted a sequence within the first exon of *FT1* (position 97 to 116 relative to the start codon, 5′→3′: TGACCTTCGGGAACAGGGCCGTGTCCAA). M1 grains were grown in the greenhouse for single-seed propagation.

From 17 different M1 lines, 2 to 3 grains were grown in a plant growth chamber under controlled LD conditions as described below. DNA was extracted from leaf material using the KingFisher Flex (ThermoFisher) and the BioSprint 96 DNA Plant Kit (QIAGEN) according to the manufacturer's instructions. To identify mutations within the CDS of *FT1*, the complete genomic sequence of *FT1* was amplified with flanking primers (fwd 5′→3′: GAAGGAAGGAGAAATGGCCG, rev 5′→3′: GATCGAGCGAGCATTAGTCA). PCR products were cleaned using the ExoSAP-IT PCR Product Cleanup Kit (ThermoFisher) and sequenced with Sanger Sequencing. Sequences were compared using MEGA-11 (Version 11.0.10, Tamura et al 2021).

Three T-DNA-free lines with homozygous single nucleotide polymorphisms were chosen for further experiments and termed *ft1.1*, *ft1.2* (in the background of GP-fast), and *ft1.3* (in the background of GP). T-DNA-free sister plants derived from the three mutant lines and that did not show a mutation event within the FT1 sequence were chosen as null segregant lines.

Growth conditions and plant phenotyping

All plants were grown in soil in controlled growth chambers under LDs (16 h light, 20 °C, PAR ∼250 µmol/m^{2}s; 8 h dark, 16 °C). Plants were grown in Einheitserde ED73 (Einheitserde Werkverband e.V.) with 7% sand and 4 g/L Osmocote Exact Hi.End 3 to 4 M, 4th generation (ICL Group Ltd.). All plants were stratified for 3–4 days at 4 °C and darkness after sowing.

GP-fast, GP, *ft1.1*, *ft1.2*, and *ft1.3* plants were grown in QuickPot 96T trays (HerkuPlast Kubern GmbH, pot volume 75 cm^3). At least 10 plants were scored per genotype. Flowering was scored as the days between the emergence of the seedling from the soil and plants reaching Zadoks' stage 49 when the awns exited the leaf sheath (Zadoks et al 1974). Plant height was measured at flowering as the distance between the soil and the flag leaf ligule of the main culm. Tiller number was counted as all secondary tillers that had emerged after the main culm at flowering, and the leaf number was determined on the main culm. Leaf width and length were measured on fully elongated leaves on the main culm as the leaf blade length (from the ligule to the leaf tip) and the maximum width of the blade. The emergence of leaves and tillers was scored every 2–3 days by visual inspection of the plants. As soon as tillers were visibly aborted (turned yellow), they were excluded from the scoring. If available, floret and grain number were determined on the main culm. This was used to calculate the spike fertility (as grains per florets). Tiller fertility was determined by dividing the number of tillers with a spike that held at least one grain by the total tiller number. The main culm abortion rate was determined by scoring whether the main culm produced a spike or not.

To test the effect of tiller number on main culm fertility, WT plants, mutant lines and null segregant lines were sown in QuickPot 96T trays (HerkuPlast Kubern GmbH, pot volume 75 cm^3). At 10 DAE, at least four (null segregant lines) or eight (*ft1* lines) plants per genotype were repotted to single 1.5 L pots, and plants were cultivated under LD conditions for phenotyping. Flowering, plant height, tiller number, and leaf number were scored as described above and the main culm abortion rate was determined for all genotypes.

Main shoot apex (MSA) development of GP, GP-fast, *ft1.1*, *ft1.2*, and *ft1.3* was monitored under LD. Every 4–13 days, the main culms of 3–4 individual plants were dissected, starting 4 DAE for GP-fast and 7 DAE for the other genotypes. Parent plants were dissected more frequently than *ft1* mutants due to the faster development. The stage of the MSA was documented using the stereo microscope Nikon SMZ18 with a Nikon DS-Fi2 camera, analyzed with the NIS-Elements Software (version 5.21.03, Nikon Instruments Europe BV), and quantified according to the Waddington scale (Waddington et al 1983). This scale rates the progression of SM initiation and the development of the most advanced floret meristem (FM) and pistil of the main inflorescence. During early development (W1.0), the MSA is vegetative, and leaf primordia are initiated. The MSA transitions to a reproductive inflorescence at the double ridge stage (W1.5 to W2.0), when SMs become visible adjacent to the leaf primordia, forming the characteristic "double ridges". Leaf primordia are suppressed, and instead, SMs are induced until approximately W5.0, which determines the maximum number of spikelets, florets and grains per spike (Digel et al 2015; Thirulogachandar and Schnurbusch 2021; Zhong et al 2021). Floral organ primordia start to differentiate at the stamen primordium stage (W3.5) when the central SM has differentiated into three stamen primordia. At W5.0, the last floral organ, the ovule, emerges.

Floral organs grow and develop into florets until anthesis and pollination at W10.0.

Inflorescence size was scored as the distance between the node of the lowest SM and the tip of the IM. The number of developing SMs, including those that had initiated FMs or developed into florets, was determined from Waddington stage W2.0 to W10.0. This data was used to calculate the inflorescence density (SMs per mm inflorescence length). The maximum SM stage (Waddington stage) was determined by plotting the number of SMs against developmental stage (Waddington Stage) or DAE and calculated with the R package segmented (version 1.6-2) as the break-point of two separate linear regressions (Muggeo 2003, 2008). SM initiation rate equals the slope of the first regression, and the FM abortion rate is the slope of the second regression. The maximum SM and final FM number were calculated with the linear models provided by segmented. Aborted FMs were calculated by subtracting the final FM number from the maximum SM number. All numbers were rounded to one decimal place.

Pollen, anther, and grain measurements

Spikes with central florets at approximately Waddington stage W10.0 were used to test pollen viability according to a modified protocol from Peterson et al (2010). Main culm spikes were harvested from at least three individual plants per genotype. Six central florets (from both sides of the two-rowed spike) were opened from each spike, and anther size was determined by measuring the length of the three anthers per floret using the software Fiji (Schindelin et al 2012). From 2 to 3 of these florets, the anthers were transferred into the staining solution (as described in Peterson et al 2010) without prior fixing. Samples were incubated for 40 min at 100 °C. Then, free pollen in the staining solution were transferred to a microscope slide. The examination was performed using a Nikon stereo microscope (Nikon SMZ18), and the images were taken with a Nikon DS-Fi2 digital camera connected to the microscope. Pollen viability was determined by visually inspecting whether pollen were stained purple (classified as viable) or stained light blue (classified as nonviable). For each floret, 60 to 400 pollen grains were classified. The viability (ratio of viable to all pollen) was averaged per floret. To determine the average pollen diameter, 10 randomly chosen fertile pollen were measured per floret, using Fiji. Numbers were averaged for each floret.

For SEM imaging, pollen were collected from anthers of GP-fast and *ft1.1* plants and transferred into a 2 mL tube with 1 mL of 1× PBS (pH 7.4). The PBS was discarded, and 1 mL fixative solution (1% glutaraldehyde, 4% paraformaldehyde, 0.03% Triton-X100, 1× PBS pH 7.4) was added under the fume hood. A vacuum was applied for 1 to 2 h at room temperature (RT) until the pollen had sunk to the bottom of the tube. The fixative was discarded and followed by three 15-minute washing steps with 1 mL of 1× PBS. The pollen were dehydrated by incubating them step-by-step in an increasing percentage of ethanol for 30 min each: Pollen were transferred to 10% EtOH first, followed by 20%, 30%, 50%, 70%, 90%, and final 100%. Next, pollen were transferred to a 1:2 hexamethyldisilazane (HMDS) solution in 100% EtOH and incubated for 20 min at RT. Subsequently, pollen were transferred to a 2:1 solution of HDMS in 100% EtOH and incubated for 20 min. Finally, pollen were transferred to 100% HMDS and left overnight in the fume hood to dry. Until imaging, pollen were stored dry. SEM images were taken at the Forschungszentrum Jülich.

Different yield parameters were measured using a MARViN ProLine (MARViTECH GmbH) and an external scale on grains from GP, GP-fast, *ft1.1*, *ft1.2*, and *ft1.3*. Per genotype, five replicates, each containing two grains from three individual plants (thus, six grains in total), were measured with the palea facing upwards. TGW, grain area, length, and width were determined. Two randomly selected grains per genotype were photographed with the palea and with the lemma facing upwards.

RNA sample preparation and RNA sequencing

GP, GP-fast, *ft1.1*, *ft1.2*, and *ft1.3* plants were sown in QuickPot 96T trays (HerkuPlast Kubern GmbH, pot volume 75 cm^3) and transferred to a plant growth chamber after stratification and cultivated under LD conditions as described above.

For RNA Sequencing, plants were sampled at three developmental stages (W2.0, W3.5, and W5.0). Samples were taken at Zeitgeber Time (ZT) 14–15, shortly before the onset of the night when *FT1* and *Ppd-H1* expression was high. Three replicates were obtained for each developmental stage and each tissue. MSAs were collected under a stereo microscope to ensure the correct developmental stage, and the MSAs of multiple plants (W2.0: 15 plants, W3.5: 5 plants, W5.0: 4 plants) were pooled for one replicate. Leaves were sampled at the same developmental stages, and the material of two different plants was pooled for one replicate. The middle section of the youngest, fully elongated leaf was sampled, resulting in some variation in leaf number across the genotypes due to the differences in development (see Table S2). All samples were immediately frozen in liquid nitrogen and stored at -80 °C.

RNA extraction was performed with the RNeasy Plant Mini Kit (QIAGEN) according to the manufacturer's instructions. Remaining DNA was removed using the RNase-Free DNase Set (QIAGEN). The quantity and quality of the RNA was determined with a Nanophotometer (Implen) and on a 1% agarose gel. Paired-end sequencing was performed by Novogene Co., Ltd using a NovaSeq PE150 platform (Illumina), resulting in 33 to 69 million reads (5–10.5 Gbp) per sample.

RNA sequencing analysis

The initial quality control of the raw reads was performed with FastQC and then summarized with MultiQC (version 1.7, Ewels et al 2016). No trimming of the reads was required. Reads were mapped against the most recent reference transcriptome BaRTv2 (Coulter et al 2022). Mapping was performed using Salmon (version 1.9.0, Patro et al 2017), and the mapping rate averaged 90.3% across samples. Genes with at least five counts per million in at least three samples across all genotypes were considered as expressed. Out of 39,434 annotated genes in the BaRT2 transcriptome reference, we identified 17,459 (44%) and 16,930 (43%) genes expressed in MSA and leaf, respectively. The 3D RNA-seq pipeline was used to calculate transcripts per million to generate PCAs (Guo et al 2021). The false discovery rate (FDR, BH adjusted) was calculated using the R package *edgeR* (Robinson et al 2010). The log2 fold change (log2FC) was calculated with a pseudo count of 1 and by pairwise comparison of each *ft1* mutant to their respective parent (*ft1.1* and *ft1.2* against GP-fast, *ft1.3* against GP). This was done individually for each tissue and developmental stage. The raw data, including all FDR values, can be found in Datasets S1 and S2.

Differentially expressed genes (DEGs) were defined for each tissue as those genes that showed significant differences in expression (FDR < 0.01) in all pairwise comparisons (*ft1.1* vs. GP-fast, *ft1.2* vs. GP-fast and *ft1.3* vs. GP). Since developmental differences were quantitative

among GP-fast, GP with low *FT1* expression and the *ft1* mutants, we used a log2FC ≥ 1 or ≤ −1 for *ft1* mutant in GP-fast background, but in *ft1.1* vs. GP-fast and *ft1.2* vs. GP-fast and no log2FC threshold was set for the comparison of *ft1.3* vs. GP. *FT1*-regulated genes were considered if they were either up- or downregulated in all *ft1* mutants at the same stage.

For additional annotation, a strict one-to-one conversion between BaRTv2 and MorexV3 gene models (Mascher et al 2021) was created for all BaRTv2 identifiers. First, the longest CDS of each gene model was selected, and the respective datasets were aligned against each other in both directions, using BLASTN (version 2.13.0+), default parameters with "-outfmt 6". The respective outputs were ordered by seqid, bitscore, evalue, and pident. A one-to-one conversion was reported when there was a reciprocal best hit between a gene model in both directions. If there was no one-to-one conversion for the remaining DEGs, they were manually curated from the remaining best-hit alignments in both directions. In addition, the MorexV3 protein sequences (Hv_Morex.pgsb.Jul2020.aa.fa) were aligned with BLASTP (version 2.13.0+) "-outfmt 6 -max_target_seqs 1" against a local BLASTP database of Araport11 (Araport11_pep_20220914_representative_gene_model, Cheng et al 2017) and the functional annotations were retrieved from Araport11_GFF3_genes_transposons.current.gff (release 2023-01-02 by TAIR).

Gene ontology (GO) term enrichment was performed using ShinyGO 0.80 (FDR cutoff 0.05) (Ge et al 2020) on DEGs, separated by tissues and into upregulated and downregulated genes. For this, MorexV3 identifiers were used as input data. Not all BaRTv2 IDs could be annotated with a MorexV3 ID, so the number of genes used for GO term enrichment was reduced by approximately 2–5% as the BaRTv2 annotation is more complete (see Tables S1, S2 for detailed numbers). The FDR cutoff for the GO term enrichment was set at 0.05. Top GO terms, including fold enrichment and FDR values, are listed in Datasets S3 and S4. Coexpression analysis was conducted using the gene expression of *FT1*-regulated genes in the leaf and MSA, respectively. Coexpression modules were identified using the WGCNA package in R with a signed hybrid network based on biweight midcorrelation (bicor, maxPOutliers = 0.05) (Langfelder and Horvath 2008). The modules were merged for MSA samples using the Dynamic Hybrid Tree Cut algorithm (cutreeDynamic) with minModuleSize = 10, cutHeight = 0.995. Module "gray" contains the genes that cannot be signed into other modules. The gene lists for each module can be found in Datasets S1 and S2. Pearson correlations between module eigengenes and traits were computed, and corresponding *P*-values were estimated using the Student asymptotic test implemented in WGCNA.

Sugar extraction from leaves and spikes

GP, GP-fast, *ft1.1*, *ft1.2*, and *ft1.3* plants were sown in QuickPot 96T trays (HerkuPlast Kubern GmbH, pot volume 75 cm^3) and transferred to plant growth chambers after stratification and cultivated under LD conditions as described above.

To measure the concentration of soluble sugars and starch in leaves, the youngest, fully elongated leaf (leaf 3 for all genotypes) was sampled 16 DAE.

To represent a full leaf, four small sections (ca. 1 cm) of the tip, base, and mid-section of the leaf were sampled into a 1.5 mL tube and frozen quickly in liquid nitrogen. Plants were sampled at ZT 0 (end of night, EON) and ZT 16 (end of day, EOD). Ten biological replicates were sampled for each genotype and time point. Each biological replicate consisted of leaf material from a single plant.

To measure the concentration of soluble sugars and starch in developing spikes, full spikes were sampled at W8.0-W8.5 and frozen quickly in liquid nitrogen. Plants were sampled at ZT 0 (EON) and 16 (EOD). Ten biological replicates were sampled for each genotype and time point. Each biological replicate consisted of 1 to 2 spikes.

To extract soluble sugars, leaves were boiled twice in 750 µL 80% EtOH at 85 °C for 45 min while shaking (1,000 rpm). The supernatant (1.5 mL) was transferred to a fresh tube and concentrated in a vacuum concentrator overnight at 35 °C and resuspended in 900 µL H_2O. The content of glucose, fructose, and sucrose was determined for each sample by subsequently adding 2.5 µg glucose-6-phosphate dehydrogenase (Roche, REF 10127671001), 0.75 U hexokinase (Roche, REF 11426362001), 5 µg glucose-6-phosphate-isomerase (Roche, REF 10128139001), and at least 50 µg invertase (Sigma-Aldrich, Cat. No. I4504) to the samples and measuring the glucose-6-phosphate-dehydrogenase-dependent NADPH accumulation at 340 nm in a microplate reader.

To extract starch, the insoluble fraction (the leaf) was dried for 60 min to remove all EtOH. The leaf was frozen in liquid nitrogen and ground using 2 mm glass beads in a TissueLyser (QIAGEN) and boiled in 800 µL 0.2 M KOH for 45 min at 90 °C while shaking (1,000 rpm). Samples were neutralized to pH 6.8 with 1 M acetic acid. Starch was digested in each sample by adding 3.6 U alpha-amylase (Sigma Aldrich, Cat. No. 10065-10G) and 2.5 U amyloglucosidase (Sigma Aldrich, Cat. No. 10115-1G-F) at 30 °C overnight. The starch amount was measured as glucose content as described above.

Statistical analyses

All statistical tests were performed using R (RStudio Team 2022). Significance between two groups in soluble sugars and starch measurement, statistic was determined by comparing GP or *ft1* mutants to GP-fast at either EOD or EON using Fisher's *F*-test for homoscedasticity, followed by Welch's *t*-statistic. Significance between more than two groups was determined using a one-way ANOVA (function *aov*) and a subsequent Tukey test (function *HSD.test* from package *agricolae*, v1.3-5), *P*-value cutoff at ≤0.05. Polynomial regressions (Loess smooth line) were calculated with a 95% confidence interval.

Accession numbers

Sequence data from this article can be found in the DataPLANT under https://doi.org/10.60534/zdm2e-8zy95.

Acknowledgments

We greatly thank Rebekka Schüller, Nina Döring, and Sabine Sommerfeld for excellent technical assistance, and Dominik Brilhaus for data management support.

Author contributions

G.H. and M.v.K. conceived and designed the experiments. G.H. genotyped and identified the *ft1* mutants, conducted plant phenotyping, sampled for RNA-seq, and analyzed and interpreted the data. T.L. assisted with sample collection and analyzed the RNAseq data. E.H.B. contributed to RNAseq analysis. T.R. extracted and analyzed carbohydrates with the help of P.W. and K.W. J.K. and G.ö.H. designed and

cloned Cas9 transformation vectors and performed the transformation and regeneration of *ft1* mutants. R.S. provided guidance, feedback, and support throughout the project. G.H. and T.L. wrote the manuscript with the help of M.v.K.

Supplementary material

Supplementary material is available at *Plant Physiology* online.

Figure S1. Nucleotide and amino acid alignment of *FT1*.

Figure S2. Effect of *FT1* on leaf development.

Figure S3. Phenotype of *ft1* mutants depending on pot size.

Figure S4. Shoot architecture of *ft1* plants.

Figure S5. Effects of *FT1* on reproductive development.

Figure S6. Formation of secondary inflorescences in the *ft1* mutants.

Figure S7. Effects of *FT1* on anther and pollen development.

Figure S8. Grain size measurements.

Figure S9. PCA and GO term enrichment for the global leaf transcriptome.

Figure S10. PCA and GO term enrichment for the global MSA transcriptome.

Figure S11. Selected DEGs representative of the major functional groups in the leaf.

Figure S12. Selected DEGs in the main shoot apex.

Figure S13. Weighted gene coexpression network analysis (WGCNA) of the *FT1*-regulated genes in the leaf and main shoot apex.

Figure S14. Effect of *FT1* on carbohydrate content in the leaf and spike.

Figure S15. Genotyping by RNA sequencing of introgression regions in GP-fast.

Figure S16. Vector map of transformation construct pGH465.

Table S1. Developmental timing and spike phenotypes of wild types and *ft1* plants.

Table S2. Overview of all leaf samples for RNA Sequencing.

Dataset S1. Transcript per million values of all genes expressed in the leaf and analyses of DEG and WGCNA.

Dataset S2. Transcript per million values of all genes expressed in the main shoot apex and analyses of DEG and WGCNA.

Dataset S3. GO term enrichment of differentially expressed genes (DEGs) in the leaf.

Dataset S4. GO term enrichment of differentially expressed genes (DEGs) in the main shoot apex.

Funding

This work was funded by the European Research Council (ERC) under the European Union's Horizon Europe research and innovation programme (PERLIFE, No. 101002085), the Deutsche Forschungsgemeinschaft (DFG) under Germany's Excellence Strategy—EXC-2048/1—Project ID: 390686111, grant KO3498/13-1, the DFG Research Unit FOR5235 "Cereal Stem Cell Systems" (CSCS) (KO 3498/16-1, AOBJ: 680652), and the IRTG 2466: *Network, exchange, and training program to understand plant resource allocation*—Project ID: 391465903.

Conflicts of interest

The authors declare no conflict of interest.

Data availability

Sequence data from this article can be found in the DataPLANT under https://doi.org/10.60534/zdm2e-8zy95.

References

Abe M *et al.* 2005. Fd, a bZIP protein mediating signals from the floral pathway integrator FT at the shoot apex. *Science*. 309:1052–1056. https://doi.org/10.1126/science.1115983.

Ahn JH *et al.* 2006. A divergent external loop confers antagonistic activity on floral regulators FT and TFL1. *EMBO J*. 25:605–614. https://doi.org/10.1038/sj.emboj.7600950.

Albani MC, Coupland G. 2010. Comparative analysis of flowering in annual and perennial plants. *Curr Top Dev Biol*. 91:323–348. https://doi.org/10.1016/S0070-2153(10)91011-9.

Balanzà V *et al.* 2018. Genetic control of meristem arrest and life span in Arabidopsis by a FRUITFULL-APETALA2 pathway. *Nat Commun*. 9:565. https://doi.org/10.1038/s41467-018-03067-5.

Banfield MJ, Brady RL. 2000. The structure of Antirrhinum centroradialis protein (CEN) suggests a role as a kinase regulator. *J Mol Biol*. 297:1159–1170. https://doi.org/10.1006/jmbi.2000.3619.

Bartlett ME, Thompson B. 2014. Meristem identity and phyllotaxis in inflorescence development. *Front Plant Sci*. 5:508. https://doi.org/10.3389/fpls.2014.00508.

Beales J, Turner A, Griffiths S, Snape JW, Laurie DA. 2007. A pseudo-response regulator is misexpressed in the photoperiod insensitive *Ppd-D1a* mutant of wheat (*Triticum aestivum L.*). TAG. Theoretical and applied genetics. *Theor Appl Genet*. 115:721–733. https://doi.org/10.1007/s00122-007-0603-4.

Benlloch R, Berbel A, Serrano-Mislata A, Madueño F. 2007. Floral initiation and inflorescence architecture: a comparative view. *Ann Bot*. 100:659–676. https://doi.org/10.1093/aob/mcm146.

Bennett T, Dixon LE. 2021. Asymmetric expansions of FT and TFL1 lineages characterize differential evolution of the EuPEBP family in the major angiosperm lineages. *BMC Biol*. 19:181. https://doi.org/10.1186/s12915-021-01128-8.

Bi X *et al.* 2019. Centroradialis interacts with *FLOWERING LOCUS T*-like genes to control floret development and grain number. *Plant Physiol*. 180:1013–1030. https://doi.org/10.1104/pp.18.01454.

Biancucci M *et al.* 2025. Mutations in HEADING DATE 1 affect transcription and cell wall composition in rice. *Plant Physiol*. 197:kiaf120. https://doi.org/10.1093/plphys/kiaf120.

Bommert P, Whipple C. 2018. Grass inflorescence architecture and meristem determinacy. *Semin Cell Dev Biol*. 79:37–47. https://doi.org/10.1016/j.semcdb.2017.10.004.

Buchmann G *et al.* 2025 Oct 31. Golden Promise-rapid, a fast-cycling barley genotype with high transformation efficiency. bioRxiv 685778. https://doi.org/10.1101/2025.10.31.685778, preprint; not peer reviewed.

Chailakhyan M. 1936. New facts in support of the hormonal theory of plant development. *Dokl Akad Nauk SSSR*. 13:79–83.

Chardon F, Damerval C. 2005. Phylogenomic analysis of the PEBP gene family in cereals. *J Mol Evol*. 61:579–590. https://doi.org/10.1007/s00239-004-0179-4.

Chen Q *et al.* 2018. *Flowering LOCUS T* mRNA is synthesized in specialized companion cells in *Arabidopsis* and Maryland Mammoth tobacco leaf veins. *Proc Natl Acad Sci U S A*. 115:2830–2835. https://doi.org/10.1073/pnas.1719455115.

Cheng C-Y *et al.* 2017. Araport11: a complete reannotation of the *Arabidopsis thaliana* reference genome. *Plant J*. 89:789–804. https://doi.org/10.1111/tpj.13415.

Corbesier L *et al.* 2007. Ft protein movement contributes to long-distance signaling in floral induction of *Arabidopsis*. *Science*. 316:1030–1033. https://doi.org/10.1126/science.1141752.

Coulter M *et al.* 2022. Bartv2: a highly resolved barley reference transcriptome for accurate transcript-specific RNA-seq quantification. *Plant J*. 111:1183–1202. https://doi.org/10.1111/tpj.15871.

Digel B *et al.* 2016. Photoperiod-H1 (*Ppd-H1*) controls leaf size. *Plant Physiol*. 172:405–415. https://doi.org/10.1104/pp.16.00977.

Digel B, Pankin A, von Korff M. 2015. Global transcriptome profiling of developing leaf and shoot apices reveals distinct genetic and environmental control of floral transition and inflorescence development in barley. *Plant Cell*. 27:2318–2334. https://doi.org/10.1105/tpc.15.00203.

Dixon LE *et al.* 2018. Developmental responses of bread wheat to changes in ambient tempera-ture following deletion of a locus that includes FLOWERING LOCUS T1. *Plant Cell Environ*. 41:1715–1725. https://doi.org/10.1111/pce.13130.

Dresselhaus T *et al.* 2025. How meristems shape plant architecture in cereals—cereal stem cell systems (CSCS) consortium. *Plant Cell*. 37: koaf150. https://doi.org/10.1093/plcell/koaf150.

Ejaz M, von Korff M. 2017. The genetic control of reproductive development under high ambient temperature. *Plant Physiol*. 173:294–306. https://doi.org/10.1104/pp.16.01275.

Ewels P, Magnusson M, Lundin S, Käller M. 2016. Multiqc: summarize analysis results for multiple tools and samples in a single report. *Bioinformatics*. 32:3047–3048. https://doi.org/10.1093/bioinformatics/btw354.

Faure S, Higgins J, Turner A, Laurie DA. 2007. The *FLOWERING LOCUS T*-like gene family in barley (*Hordeum vulgare*). *Genetics*. 176:599–609. https://doi.org/10.1534/genetics.106.069500.

Fichtner F, Lunn JE. 2021. The role of trehalose 6-phosphate (Tre6P) in plant metabolism and development. *Annu Rev Plant Biol*. 72:737–760. https://doi.org/10.1146/annurev-arplant-050718-095929.

Finnegan EJ *et al.* 2018. Zebularine treatment is associated with deletion of FT-B1 leading to an increase in spikelet number in bread wheat. *Plant Cell Environ*. 41:1346–1360. https://doi.org/10.1111/pce.13164.

Ge SX, Jung D, Yao R. 2020. Shinygo: a graphical gene-set enrichment tool for animals and plants. *Bioinformatics*. 36:2628–2629. https://doi.org/10.1093/bioinformatics/btz931.

Gerasimova SV *et al.* 2018. Targeted genome modification in protoplasts of a highly regenerable Siberian barley cultivar using RNA-guided Cas9 endonuclease. *Vavilovskii Zhurnal Genet Selektsii*. 22:1033–1039. https://doi.org/10.18699/VJ18.447.

Gol L, Haraldsson EB, von Korff M. 2021. Ppd-H1 integrates drought stress signals to control spike development and flowering time in barley. *J Exp Bot*. 72:122–136. https://doi.org/10.1093/jxb/eraa261.

Gol L, Tomé F, von Korff M. 2017. Floral transitions in wheat and barley: interactions between photoperiod, abiotic stresses and nutrient status. *J Exp Bot*. 68:1399–1410. https://doi.org/10.1093/jxb/erx055.

González-Suárez P, Walker CH, Bennett T. 2023. Flowering LOCUS T mediates photo-thermal timing of inflorescence meristem arrest in Arabidopsis thaliana. *Plant Physiol*. 192:2276–2289. https://doi.org/10.1093/plphys/kiad163.

Guo W *et al.* 2021. 3d RNA-seq: a powerful and flexible tool for rapid and accurate differential expression and alternative splicing analysis of RNA-seq data for biologists. *RNA Biol*. 18:1574–1587. https://doi.org/10.1080/15476286.2020.1858253.

Halliwell J *et al.* 2016. Systematic investigation of FLOWERING LOCUS T-like Poaceae gene families identifies the short-day expressed flowering pathway gene, TaFT3 in wheat (Triticum aestivum L.). *Front Plant Sci*. 7:857. https://doi.org/10.3389/fpls.2016.00857.

Hanzawa Y, Money T, Bradley D. 2005. A single amino acid converts a repressor to an activator of flowering. *Proc Natl Acad Sci U S A*. 102: 7748–7753. https://doi.org/10.1073/pnas.0500932102.

John S *et al.* 2022 Oct 27. Transcription factor HSFA7b controls ethylene signaling and meristem maintenance at the shoot apical meristem during thermomemory. bioRxiv 513826. https://doi.org/10.1101/2022.10.26.513826, preprint; not peer reviewed.

John S *et al.* 2024. The transcription factor HSFA7b controls thermomemory at the shoot apical meristem by regulating ethylene biosynthesis and signaling in Arabidopsis. *Plant Comm*. 5:100743. https://doi.org/10.1016/j.xplc.2023.100743.

Jones H *et al.* 2008. Population-based resequencing reveals that the flowering time adaptation of cultivated barley originated east of the Fertile Crescent. *Mol Biol Evol*. 25:2211–2219. https://doi.org/10.1093/molbev/msn167.

Kardailsky I *et al.* 1999. Activation tagging of the floral inducer *FT*. *Science*. 286:1962–1965. https://doi.org/10.1126/science.286.5446.1962.

Kumar R *et al.* 2023. Genetic architecture of source–sink-regulated senescence in maize. *Plant Physiol*. 193:2459–2479. https://doi.org/10.1093/plphys/kiad460.

Lan T *et al.* 2025. PHOTOPERIOD 1 enhances stress resistance and energy metabolism to promote spike fertility in barley under high ambient temperatures. *Plant Physiol*. 197:kiaf118. https://doi.org/10.1093/plphys/kiaf118.

Langfelder P, Horvath S. 2008. WGCNA: an R package for weighted correlation network analysis. *BMC Bioinform*. 29:559. https://doi.org/10.1186/1471-2105-9-559.

Li C, Lin H, Dubcovsky J. 2015. Factorial combinations of protein interactions generate a multiplicity of florigen activation complexes in wheat and barley. *Plant J*. 84:70–82. https://doi.org/10.1111/tpj.12960.

Li K *et al.* 2021. Interactions between SQUAMOSA and SHORT VEGETATIVE PHASE MADS-box proteins regulate meristem transitions during wheat spike development. *Plant Cell*. 33:3621–3644. https://doi.org/10.1093/plcell/koab243.

Lv B *et al.* 2014. Characterization of *FLOWERING LOCUS T1 (FT1)* gene in Brachypodium and wheat. *PLoS One*. 9:e94171. https://doi.org/10.1371/journal.pone.0094171.

Lv X, Zhang Y, Zhang Y, Fan S, Kong L. 2020. Source-sink modifications affect leaf senescence and grain mass in wheat as revealed by proteomic analysis. *BMC Plant Biol*. 20:257. https://doi.org/10.1186/s12870-020-02447-8.

Marthe C, Kumlehn J, Hensel G. 2015. Barley (Hordeum vulgare L.) transformation using immature embryos. In: Wang K, editor. *Agrobacterium protocols, volume 1, methods in molecular biology*, Vol. 1223, Chapter 6. Springer Science+Business Media. p. 71–83.

Mascher M *et al.* 2021. Long-read sequence assembly: a technical evaluation in barley. *Plant Cell*. 33:1888–1906. https://doi.org/10.1093/plcell/koab077.

Melzer S *et al.* 2008. Flowering-time genes modulate meristem determinacy and growth form in Arabidopsis thaliana. *Nat Genet*. 40: 1489–1492. https://doi.org/10.1038/ng.253.

Miryeganeh M. 2021. Plants' epigenetic mechanisms and abiotic stress. *Genes (Basel)*. 12:1106. https://doi.org/10.3390/genes12081106.

Muggeo VMR. 2003. Estimating regression models with unknown breakpoints. *Stat Med*. 22:3055–3071. https://doi.org/10.1002/sim.1545.

Muggeo VMR. 2008. Segmented: an R package to fit regression models with broken-line relationships. *R News*. 8:20–25.

Mulki MA, Bi X, von Korff M. 2018. *Flowering LOCUS T3* controls spikelet initiation but not floral development. *Plant Physiol*. 178:1170–1186. https://doi.org/10.1104/pp.18.00236.

Olas JJ *et al.* 2021. Primary carbohydrate metabolism genes participate in heat-stress memory at the shoot apical meristem of Arabidopsis thaliana. *Mol Plant*. 14:1508–1524. https://doi.org/10.1016/j.molp.2021.05.024.

Park SJ *et al.* 2014. Optimization of crop productivity in tomato using induced mutations in the florigen pathway. *Nat Genet*. 46:1337–1342. https://doi.org/10.1038/ng.3131.

Patro R, Duggal G, Love MI, Irizarry RA, Kingsford C. 2017. Salmon provides fast and bias-aware quantification of transcript expression. *Nat Methods*. 14:417–419. https://doi.org/10.1038/nmeth.4197.

Paul MJ, Foyer C. 2001. Sink regulation of photosynthesis. *J Exp Bot*. 52: 1383–1400. https://doi.org/10.1093/jexbot/52.360.1383.

Peterson R, Slovin JP, Chen C. 2010. A simplified method for differential staining of aborted and non-aborted pollen grains. *Int J Plant Biol*. 1: 13. https://doi.org/10.4081/pb.2010.e13.

Pieper R, Tomé F, von Korff M. 2021. *FLOWERING LOCUS T4 (HvFT4)* delays flowering and decreases floret fertility in barley. *J Exp Bot*. 180. https://doi.org/10.1093/jxb/eraa466.

Robinson MD, McCarthy DJ, Smyth GK. 2010. Edger: a Bioconductor package for differential expression analysis of digital gene expression data. *Bioinformatics*. 26:139–140. https://doi.org/10.1093/bioinformatics/btp616.

RStudio Team. 2022. *RStudio: integrated development for R. RStudio [computer software]*. PBC. http://www.rstudio.com/

Sang N, Ma B, Liu H, Feng T, Huang X. 2025. CRISPR/Cas9-mediated GhFT-targeted mutagenesis prolongs indeterminate growth and alters plant architecture in cotton. *Plant Sci*. 352:112374. https://doi.org/10.1016/j.plantsci.2024.112374.

Schindelin J *et al.* 2012. Fiji: an open-source platform for biological-image analysis. *Nat Methods*. 9:676–682. https://doi.org/10.1038/nmeth.2019.

Sewelam N, Kazan K, Schenk PM. 2016. Global plant stress signaling: reactive oxygen species at the cross-road. *Front Plant Sci*. 7:187. https://doi.org/10.3389/fpls.2016.00187.

Shanmugaraj N *et al.* 2023. Multilayered regulation of developmentally programmed pre-anthesis tip degeneration of the barley inflorescence. *Plant Cell*. 35:3973–4001. https://doi.org/10.1093/plcell/koad164.

Shaw LM *et al.* 2019. *Flowering LOCUS T2* regulates spike development and fertility in temperate cereals. *J Exp Bot*. 70:193–204. https://doi.org/10.1093/jxb/ery350.

Shaw LM, Turner AS, Herry L, Griffiths S, Laurie DA. 2013. Mutant alleles of *Photoperiod-1* in wheat (*Triticum aestivum L.*) that confer a late flowering phenotype in long days. *PLoS One*. 8:e79459. https://doi.org/10.1371/journal.pone.0079459.

Tamaki S, Matsuo S, Wong HL, Yokoi S, Shimamoto K. 2007. Hd3a protein is a mobile flowering signal in rice. *Science*. 316:1033–1036. https://doi.org/10.1126/science.1141753.

Tamura K, Stecher G, Kumar S. 2021. Mega11: molecular evolutionary genetics analysis version 11. *Mol Biol Evol*. 38:3022–3027. https://doi.org/10.1093/molbev/msab120.

Taoka K-I *et al.* 2011. 14-3-3 proteins act as intracellular receptors for rice Hd3a florigen. *Nature*. 476:332–335. https://doi.org/10.1038/nature10272.

Thirulogachandar V, Schnurbusch T. 2021. 'Spikelet stop' determines the maximum yield potential stage in barley. *J Exp Bot*. 72:7743–7753. https://doi.org/10.1093/jxb/erab342.

Trevaskis B *et al.* 2007. Short vegetative phase-like MADS-box genes inhibit floral meristem identity in barley. *Plant Physiol*. 143:225–235. https://doi.org/10.1104/pp.106.090860.

Turner A, Beales J, Faure S, Dunford RP, Laurie DA. 2005. The pseudo-response regulator *Ppd-H1* provides adaptation to photoperiod in barley. *Science*. 310:1031–1034. https://doi.org/10.1126/science.1117619.

Waddington SR, Cartwright PM, Wall PC. 1983. A quantitative scale of spike initial and pistil development in barley and wheat. *Ann Bot*. 51: 119–130. https://doi.org/10.1093/oxfordjournals.aob.a086434.

Walla A *et al.* 2020. An acyl-CoA N-acyltransferase regulates meristem phase change and plant architecture in barley. *Plant Physiol*. 183: 1088–1109. https://doi.org/10.1104/pp.20.00087.

Wang B, Smith SM, Li J. 2018. Genetic regulation of shoot architecture. *Annu Rev Plant Biol*. 69:437–468. https://doi.org/10.1146/annurev-arplant-042817-040422.

Wigge PA *et al.* 2005. Integration of spatial and temporal information during floral induction in *Arabidopsis*. *Science*. 309:1056–1059. https://doi.org/10.1126/science.1114358.

Yan L *et al.* 2006. The wheat and barley vernalization gene *VRN3* is an orthologue of *FT*. *Proc Natl Acad Sci U S A*. 103:19581–19586. https://doi.org/10.1073/pnas.0607142103.

Zadoks JC, Chang TT, Konzak CF. 1974. A decimal code for the growth stages of cereals. *Weed Res*. 14:415–421. https://doi.org/10.1111/j.1365-3180.1974.tb01084.x.

Zhong J *et al.* 2021. INTERMEDIUM-Mencodes an HvAP2L-H5 ortholog and is required for inflorescence indeterminacy and spikelet determinacy in barley. *Proc Natl Acad Sci*. 118. https://doi.org/10.1073/pnas.2011779118